RSC Advances

PAPER

View Article Online
View Journal | View Issue

Cite this: *RSC Adv.*, 2025, **15**, 35479

Enhancing wastewater treatment: a study on steam explosion-biochar derived from Chinese herbal medicine residue for NOR adsorption

Dong Guo,†[a] Pengwei Li,†[a] Lin Meng,[a] Ziheng Zhao,[ac] Hang Su,[a] Weisheng Feng[a] and Zhijuan Zhang *[ab]

Steam explosion technology is gaining attention as an economical, efficient, and eco-friendly industrial pretreatment method. This study used Astragali Radix (AR) residue, activated by steam explosion, to create biochar for removing norfloxacin (NOR) from water. The prepared biochar was analyzed using various techniques, revealing ASB4's rich microporous and mesoporous structure with a surface area of 512 m^2 g^{-1}. Kinetic studies showed rapid NOR adsorption best described by the PSO model, with a maximum capacity of 345.7 mg g^{-1} at 298 K, according to Langmuir models. Thermodynamic analysis confirmed that the adsorption was exothermic and spontaneous. The adsorption process is mainly driven by pore filling, followed by hydrogen bonding (13.4%), and electrostatic interactions (7.5%), with π–π interactions (3.6%) being the least significant. Moreover, the utilization of response surface modeling (RSM) facilitated the optimization of the adsorption capacity of NOR, yielding a maximum removal capacity of 324 mg g^{-1} at 298 K, an initial concentration of 200 mg L^{-1}, and a pH of 7.83. Economically, the biochar material offers cost benefits with a payback of 1.87 $ per kg. ASB4 demonstrated excellent stability and reusability, retaining a high NOR removal rate even after five cycles. This study highlights the potential of converting AR residues into activated carbons, aligning with circular economy principles and improving wastewater treatment efficiency.

Received 11th July 2025
Accepted 18th September 2025

DOI: 10.1039/d5ra04964d

rsc.li/rsc-advances

1. Introduction

Rapid industrialization and the growth of medical systems have increased the use of toxic organic pollutants like dyes, antibiotics, and pesticides, which often contaminate water due to poor treatment and accidental leaks, harming ecosystems.[1,2] NOR, a widely used quinolone antibiotic, is recognized for its potent antibacterial properties and minimal side effects.[3] Nonetheless, its high stability and low biodegradability result in significant quantities of NOR and its metabolites being discharged into the environment post-use, posing potential risks to both environmental and human health.[4] Consequently, there is an urgent need for effective strategies to eliminate NOR.

Adsorption is a promising solution due to its simplicity, cost-effectiveness, and sustainability. Various materials, including graphene oxide,[5] carbon nanotubes,[6,7] metal–organic frameworks,[8,9] clays,[10] and bilayer hydroxides,[11] have been employed as adsorbents. However, certain limitations exist, such as high costs, low adsorption efficiencies, and the potential for secondary environmental pollution. Conversely, activated carbon presents several advantages, including environmental friendliness, accessibility, cost-effectiveness, and efficiency.[12] Consequently, the production of carbon-based adsorbents from biomass has gained significant traction over the past few decades.

To enhance the adsorption capacity, biochar is often modified physically and chemically, using agents like NaOH, KOH, $ZnCl_2$, and H_3PO_4. While chemical activation can cause equipment corrosion and pollution, physical activation is more sustainable and cost-effective. Common physical activation methods like green carbonization,[13] ball milling[14,15] and steam explosion[16] are used to produce adsorbents. Kasturi Poddar *et al.*[17] achieved a 69.8 mg g^{-1} adsorption capacity for NOR using biochar from waste coffee grounds, while Luo *et al.*[18] used longan seed to produce activated carbon with a 76.6 mg g^{-1} capacity. Despite being eco-friendly, these methods often yield materials with low surface area and adsorption capacity. Steam explosion, originally developed for fiberboard production, is a sustainable, efficient, and economical thermo-processing method that requires no toxic chemicals and involves low capital investment. It's recognized as a cost-effective and environmentally friendly pretreatment for industrial-scale applications, extensively studied for lignocellulosic biomass. Operating

[a]*College of Pharmacy, Henan University of Chinese Medicine, Zhengzhou 450046, China. E-mail: zhangyan0204@126.com*
[b]*Collaborative Innovation Center of Research and Development on the Whole Industry Chain of Yu-Yao, Zhengzhou 450046, Henan Province, China*
[c]*Shangqiu Municipal Hospital, Shangqiu 476100, China*
† These authors contributed equally to this work.

at 160–260 °C with rapid pressure reduction, it enhances adsorbent production by increasing surface area through hemicellulose degradation and lignin softening.[19,20]

AR, a traditional Chinese medicine, treats conditions like qi deficiency and has anti-cancer, antiviral, and immunomodulatory properties.[21,22] After extraction, AR residue, rich in cellulose, hemicellulose, and lignin, can serve as a precursor for activated carbon production.[23] This study developed a biochar adsorbent using steam-exploded AR residue to address water antibiotic pollution. The adsorption properties of the prepared biochar material, targeting NOR, were analyzed using FTIR, SEM, BET, XRD and XPS, considering factors like pH, temperature, NOR concentration, and contact time. The adsorbent's reusability, stability, and economic viability were also assessed.

2. Experimental section

2.1 Materials and methods

AR residue was provided by Lingrui Pharmaceutical Co., Ltd in Henan province, China. NaOH (96%), HCl (37%), KCl (99.5%), NaCl (99.5%), $CaCl_2$ (96%), Na_2CO_3 (99.5%), $NaNO_3$ (98%), Na_2SO_4 (99%) and NaBr (99%) were all purchased from J&K Scientific Reagent Company. $ZnCl_2$ (98%), $NaHCO_3$ (99.8%) and $CuCl_2$ (96%) were purchased from Shanghai Macklin Biochemical Co., Ltd. NOR (M_w = 319.33 g mol^{-1}, 98%) and $FeCl_3 \cdot 6H_2O$ (99%) purchased in Shanghai Aladdin Biochemical Technology Co., Ltd. The above reagents are all analytical grade and used without further purification.

2.2 Synthesis of ASBs biochars

2 g of washed, air-dried and sieved AR residue was directly put into a tube furnace for pyrolysis at 900 °C, and the product was named ARB. 4 g of clean AR residue was put into a reaction kettle filled with 60 mL of distilled water, stirred well and left for 12 h. Secure the container to the unit, then fill it with N_2 to the initial target pressure (2, 3 and 4 MPa, respectively). Then, the internal temperature of the reactor was raised to 160 °C at a rate of 8 °C min^{-1} and kept for 5 min. After that, the sample was taken out and dried. The material was transferred to the tube furnace for pyrolysis under N_2 atmosphere at 900 °C with a heating rate of 5 °C min^{-1}, maintain for 80 min. Then, it was washed with ultra-pure water to neutral. The obtained biochar was dried at 105 °C for 12 h, and the product was named as ASBX (X = 2, 3 and 4). The characterization process is comprehensively detailed in Text S1.

2.3 Adsorption studies

Batch adsorption experiments are used to examine the effect of solution pH (2–12), adsorption time (0–1440 min), and NOR initial concentration (10–200 mg L^{-1}). 5 mg of ASB4 was initially added to 10 mL NOR solution with different concentrations (10, 50, 100 mg L^{-1}), and equal portions were continuously taken at 298 K for 1440 min. The NOR adsorption kinetics was analyzed using four different kinetic models, like pseudo-first order (PFO), pseudo-second order (PSO), Elovich and intra-particle diffusion. Isotherm and thermodynamic studies were conducted at 298 K, 308 K, 318 K and 328 K, respectively. Adsorption isotherm models used included Langmuir, Freundlich, and Sips model. Its thermodynamic parameters (ΔG, ΔS and ΔH) are determined using the van der Hoff equations. The adsorption kinetics, isotherms, and thermodynamics are calculated using the equations provided in Table S1. Adsorption experiments were performed three times for each study. Detailed calculations pertaining to the adsorption capacity and removal rate are provided in Text S2.

2.4 NOR adsorption mechanisms by ASB4

This study conducted competitive adsorption experiments to quantify the roles of hydrogen bonding, π–π interactions, and electrostatic interactions in NOR adsorption onto ASB4.[24–26] Urea, with its hydrogen-donating and accepting groups, disrupted hydrogen bonds, while naphthalene interfered with π–π interactions. Sodium chloride (NaCl) was used to examine electrostatic interactions. Specifically, 5 mg of ASB4 was added to NOR solutions with varying concentrations of urea (0.5–5 M), naphthalene (50–200 mg L^{-1}), and NaCl (0.01–0.1 M). After 24 h at 298 K, residual NOR was measured using UV spectrophotometry.

2.5 Effect of coexisting ions and antibiotics on NOR adsorption

In this study, Na^+, K^+, Ca^{2+}, Cu^{2+}, Fe^{3+}, Zn^{2+}, CO_3^{2-}, HCO_3^-, Br^-, NO_3^-, SO_4^{2-} and other common competitive ions were added to evaluate the competitive adsorption effect of the prepared biochar on NOR removal. Furthermore, this study also examined the impact of co-existing antibiotics (50 mg L^{-1}), specifically ciprofloxacin (CIP), enoxacin (ENX), tetracycline (TC), and oxytetracycline (OTC), on the adsorption of NOR, which was maintained at a concentration of 50 mg L^{-1}.

2.6 Regeneration properties

In each cycle, the ASB4 that has adsorbed NOR was thoroughly washed with a 1 M NaOH solution. After drying in the oven, the recovered biochar is used to explore its reusability and stability in the next cycle.

2.7 Response surface methodology (RSM) analysis

RSM analysis employs statistical methods to model relationships between independent variables and responses, creating regression equations and optimizing variables with minimal experiments. This study focused on initial concentration, temperature, and pH as variables. The relationship between adsorption capacity and these encoded variables (initial TC concentration, temperature, and solution pH) in RSM is described by an empirical quadratic polynomial, as presented in eqn (1).

$$y = a_0 + \sum a_i X_i + \sum a_{ij} X_i X_j + \sum a_{ii} X_i^2 \quad (1)$$

where y is the predicted response (adsorption capacity), i, j, X_i and X_j are the variables, a_0 is the constant, a_i is the linear coefficient, a_{ij} is the interaction coefficient, and a_{ii} is the

quadratic coefficient, respectively. Finally, to clarify the best adsorption conditions, multi-factor analysis of variance and quadratic regression are used to determine the influence of each variable on the removal rate.[27,28]

3. Results and discussion

3.1 Characterization of the prepared biochars

Fig. 1a and b present the N_2 adsorption–desorption isotherm at 77 K and NLDFT pore size distribution of the prepared biochar. The isotherms clearly demonstrated type IV isotherms with H3 hysteresis loops, suggesting their mesoporous structures.[29] The pore size distribution of the biochar prior to steam explosion was primarily concentrated within the 1.3–4 nm range, aligning with the findings from the N_2 adsorption–desorption isotherm (Fig. 1b and Table 1). Moreover, increasing the steam explosion pressure led to a significant enhancement in both the S_{BET} and pore volume of the synthesized biochar. The ASB4 sample exhibited the highest S_{BET} (512 m^2 g^{-1}) and the largest V_{total} (0.534 cm^3 g^{-1}), indicating that the high-pressure steam impact during the explosion process progressively disrupted the cell wall of AR residue. This disruption facilitated the degradation of cellulose and lignin, thereby promoting the formation of pore structures on the surface during pyrolysis.[20] Under identical pyrolysis conditions, increasing the initial filling pressure of steam explosion can enhance the development of pore structures. These stratified pore structures are beneficial for the transport of adsorbed pollutants, achieving effective adsorption.[30]

The micromorphology of the synthesized ASB4 was examined using SEM (Fig. 1c–f). Fig. 1c exhibits a relatively flat surface with minor particles and pores. Fig. 1d shows a considerably rougher texture featuring larger particles with non-uniform distribution. Fig. 1e presents a more complex surface morphology, characterized by distinct lamellar and granular structures. Fig. 1f displays a highly intricate

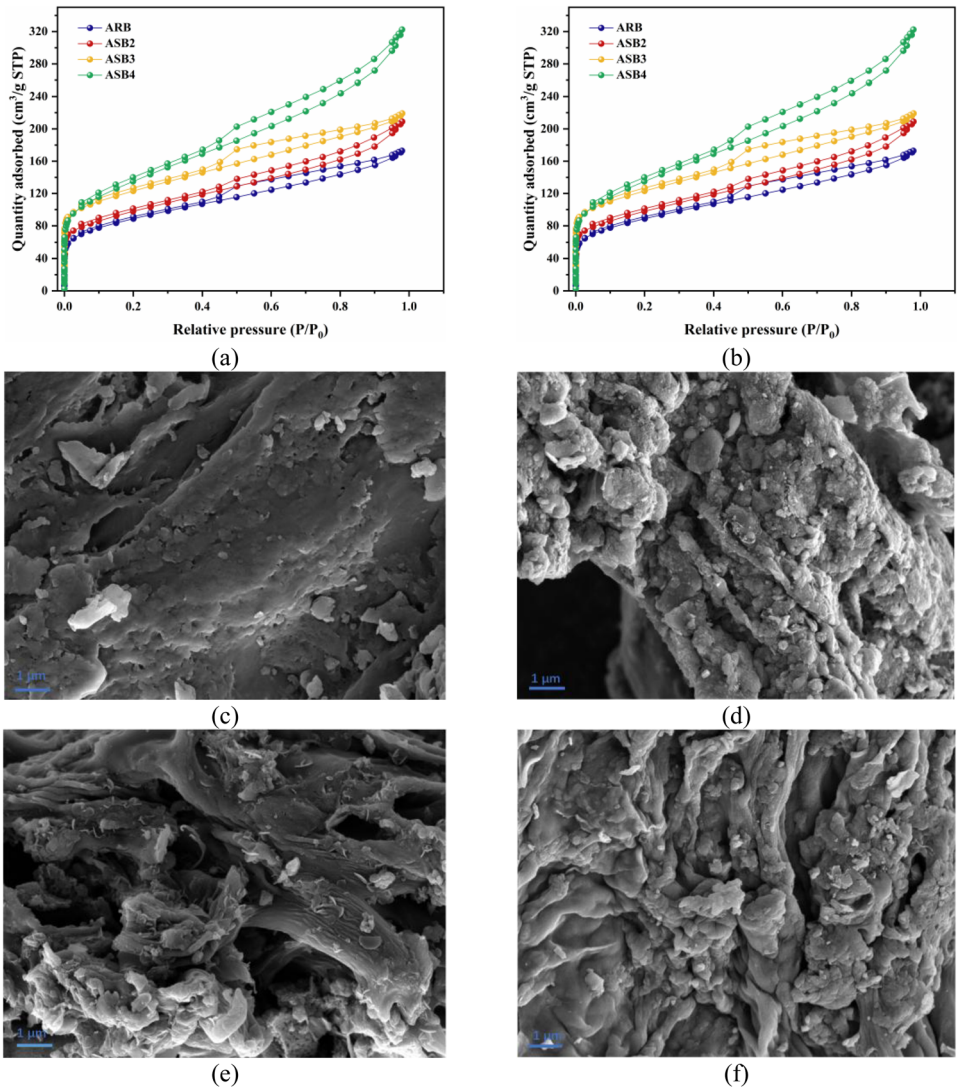

Fig. 1 (a) N_2 adsorption–desorption isotherms of biochar materials at 77 K, (b) the pore size distributions of biochar materials based on nonlocal density functional theory (NLDFT), SEM images of prepared biochars (c) ARB, (d) ASB2, (e) ASB3, (f) ASB4.

Table 1 Porous structure parameters of the synthesized biochars by steam explosion

Samples	S_{BET} ($m^2\ g^{-1}$)	$S_{Langmuir}$ ($m^2\ g^{-1}$)	V_{Micro} ($cm^3\ g^{-1}$)	V_{Total} ($cm^3\ g^{-1}$)	Average pore diameter (nm)
ARB	314	426	0.060	0.267	3.41
ASB2	274	402	0.029	0.290	3.53
ASB3	333	481	0.048	0.294	4.23
ASB4	512	745	0.066	0.534	4.16

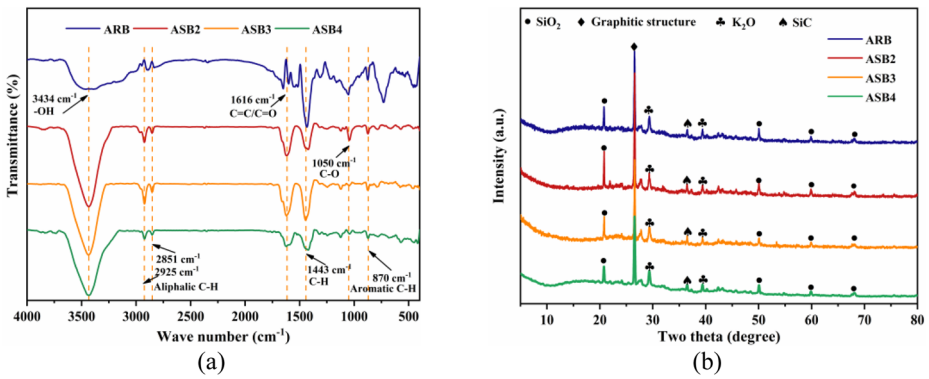

Fig. 2 Comparison of FT-IR spectra (a) and XRD (b) of biochar materials.

architecture with pronounced layered and particulate features, along with denser interparticle connectivity. In addition, distinct porous structures can be observed in Fig. 1f, which provide active sites for the adsorption of NOR.[31]

Fig. 2a shows the FT-IR spectra of ARB, ASB2, ASB3 and ASB4 materials. The spectral peaks at 3434 cm^{-1} are attributed to the stretching vibration of OH– groups in cellulose,[32] while the peaks at 2925 cm^{-1} and 2851 cm^{-1} correspond to the stretching vibrations of CH_2 groups.[33] The peaks at 1616 cm^{-1} are associated with the stretching vibrations of C=C/C=O bonds in lignin or hemicellulose.[34] Additionally, the peak at 1443 cm^{-1} is attributed to the in-plane bending vibration of C–H in cellulose, the peak at 1050 cm^{-1} is linked to the stretching vibrations in cellulose and C–O groups,[35] and the peak at 870 cm^{-1} is ascribed to the stretching vibration of C–H on the benzene ring. The increased intensity of the –OH peak following steam explosion is due to the disruption of the cellulose structure, leading to greater exposure of OH groups. Fig. 2b presents the XRD patterns of the four samples. The diffraction peaks observed at $2\theta = 20.7°$, 50.1°, 59.8° and 67.6° are attributed to the (100), (112), (121), and (122) crystallographic planes of SiO_2, respectively, while the peak at $2\theta = 26.5°$ corresponds to the (002) plane of graphene carbon. This indicates that the sample retains its structural integrity following steam explosion treatment. Elemental analysis (EA) results reveal a sustantial increase in the carbon content of the prepared biochar compared to the ARB sample (Table 2). This increase is primarily attributed to the steam explosion treatment, which significantly enhances the exposure of cellulose in the residual material. Under elevated temperature, this exposure facilitates chemical processes such as dehydration, decarboxylation, and hydroxylation, thereby increasing the carbon content. Furthermore, the reductions in the H/C, O/C, and (N + O)/C ratios indicated an increase in the aromaticity and decreases in the polarity and hydrophilicity of the biochar.

Table 2 Elemental composition of prepared biochar

Samples	C (%)	H (%)	O (%)	N (%)	S (%)	H/C	O/C	(O + N)/C
ARB	68.34	0.51	6.88	0.60	0.15	0.007	0.10	0.11
ASB2	71.71	0.39	5.78	0.52	0.13	0.005	0.08	0.09
ASB3	78.88	0.43	7.21	0.59	0.28	0.005	0.09	0.10
ASB4	82.68	0.58	6.82	1.11	0.12	0.007	0.08	0.09

3.2 Adsorption performance

3.2.1 Selection of adsorbents. As shown in Fig. S1, under identical conditions, ASB4 exhibited the highest adsorption capacity for NOR, being 1.23, 1.37, and 1.13 times greater than that of ARB, ASB2, and ASB3, respectively. Subsequently, ASB4 was selected for subsequent experiments.

3.2.2 Effects of solution pH. The initial solution pH affects NOR's structure and the adsorbent's surface chemistry, influencing biochar's NOR adsorption capacity. The adsorbent's electrochemical properties were assessed using the point of zero charge (pH_{pzc}), found to be 3.51 for ASB4 and 3.07 for ARB (Fig. 3a). At 200 mg L^{-1} and pH 2–8, ASB4's adsorption efficiency for NOR increased, reaching over 80% removal (Fig. 3b). NOR's dissociation constants are pK_a 6.22 and 8.51, meaning its cationic below pH 6.22, amphoteric between 6.22 and 8.51, and anionic above 8.51. When pH is between 3.51 and 8.51, negatively charged ASB4 strongly interacts with NOR^+ and NOR^-. Above pH 8.51, electrostatic repulsion between ASB4 and NOR-

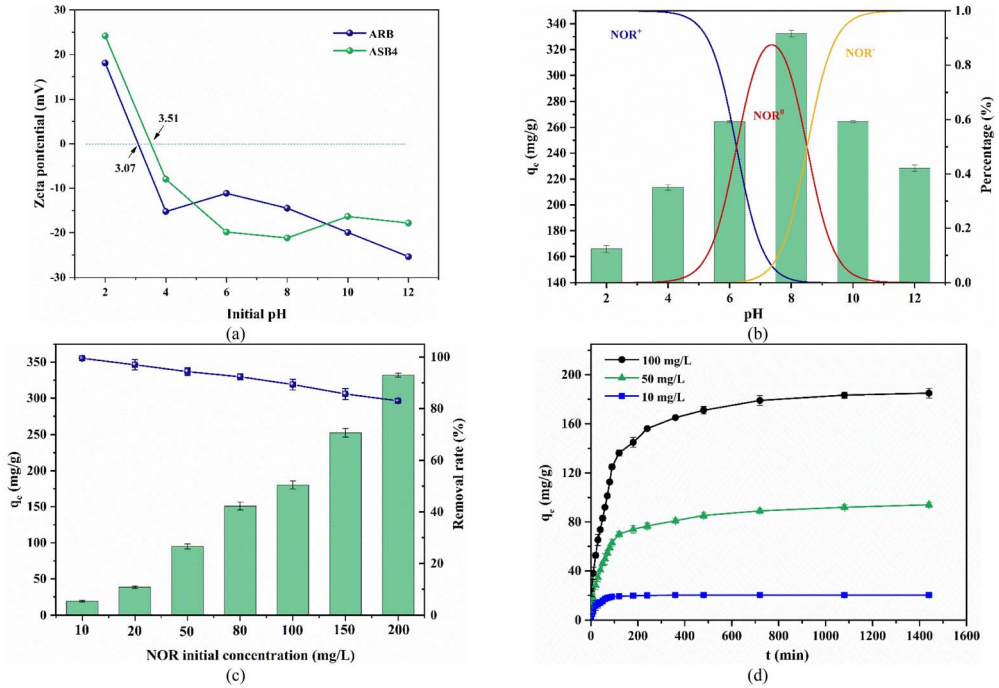

Fig. 3 (a) Zeta potentials and adsorption performance (b) adsorption of ASB4 at different pH values (pH 2–12). (c) Influence of the NOR concentration. (d) Effect of exposure time at low concentrations (pH = 8).

reduces affinity, resulting in decrease of the removal efficiency of NOR. Despite the variation in NOR removal rates across different pH levels, ASB4 remains practically applicable in actual water bodies within a wide pH range of 2–12. Furthermore, given that the maximum adsorption capacity was achieved at a pH of 8, all subsequent experiments were conducted under this pH condition.

3.2.3 Effect of initial NOR concentration and adsorption time. Fig. 3c illustrates that the adsorption capacity of ASB4 increased from 19.1 mg g^{-1} to 332 mg g^{-1} when the initial NOR

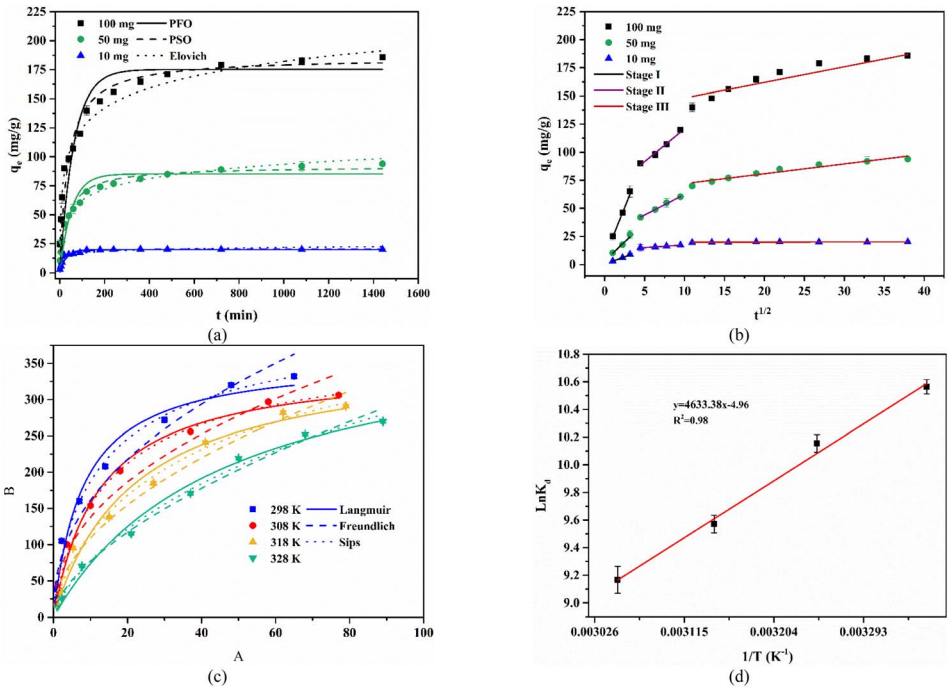

Fig. 4 (a) PFO, PSO and Elovich adsorption kinetics models of NOR adsorption by ASB4; (b) IPD adsorption kinetic of NOR adsorption by ASB4; (c) experimental and fitted adsorption isotherms of NOR on ASB4; (d) thermodynamics plot for adsorption of NOR on ASB4 (pH = 8).

Table 3 PFO, PSO and Elovich adsorption kinetics parameters of NOR adsorption on ASB4 biochar

NOR solution ($mg\ L^{-1}$)	PFO				PSO			Elovich		
	$q_{e,exp}$ ($mg\ g^{-1}$)	$q_{e,cal}$ ($mg\ g^{-1}$)	k_1 (min^{-1})	R^2	$q_{e,cal}$ ($mg\ g^{-1}$)	k_2 (min^{-1})	R^2	α ($mg\ g^{-1}\ min^{-1}$)	β	R^2
10	20.07	19.85	0.02	0.86	20.57	1.5×10^{-3}	0.95	2.738	0.287	0.87
50	94.32	85.23	0.02	0.92	91.85	3.2×10^{-4}	0.98	1.988	0.070	0.93
100	185.67	175.18	0.03	0.94	185.40	4.2×10^{-3}	0.98	2.127	0.088	0.92

Table 4 IPD adsorption kinetics parameters of NOR adsorption on ASB4 biochar

NOR solution ($mg\ L^{-1}$)	First liner segment			Second liner segment			Third liner segment		
	$k_{id,1}$ ($mg\ g^{-1}\ min^{-0.5}$)	$C_{i,1}$ ($mg\ g^{-1}$)	R^2	$k_{id,2}$ ($mg\ g^{-1}\ min^{-0.5}$)	$C_{i,2}$ ($mg\ g^{-1}$)	R^2	$k_{id,3}$ ($mg\ g^{-1}\ min^{-0.5}$)	$C_{i,3}$ ($mg\ g^{-1}$)	R^2
10	2.63	0.30	0.98	0.48	0.48	0.99	0.02	19.56	0.98
50	6.73	3.31	0.95	3.66	25.79	0.99	0.88	63.29	0.91
100	17.67	6.67	0.99	5.84	62.47	0.97	1.38	134.37	0.93

concentration was raised from 10 mg L^{-1} to 200 mg L^{-1}. However, the removal efficiency dropped from 99.5% to 83%, primarily due to the limited number of active sites available on ASB4. Given low NOR levels in water, we studied contact time effects at low concentrations (Fig. 3d). Below 100 mg L^{-1}, adsorption capacity rises quickly in the first 100 min and stabilized by 200 min.

3.2.4 Adsorption kinetics. The adsorption kinetics of NOR by ASB4 are illustrated in Fig. 4a and b, with the corresponding fitting parameters listed in Table 3 and 4. In the first 100 min, the NOR adsorption capacity increased quickly with contact time, then slowed until reaching equilibrium. This process has two phases: fast and slow adsorption. Initially, sufficient active sites are available, but they become occupied over time, leading to saturation. The PSO model fits the adsorption kinetics of NOR on ASB4 better than the PFO and Elovich models at low concentrations, indicating chemisorption as the primary mechanism. Furthermore, the q values from the PSO model match experimental results, highlighting its effectiveness at low concentrations.

For IPD model, initially, the intraparticle diffusion rate constant k_{d1} is much higher than k_{d2} and k_{d3}, indicating NOR molecules primarily diffuse to the ASB4 surface. As NOR molecules enter activated carbon pores, the adsorption process progresses to the second and third stages.[36] All C values of NOR are above 0, with $C_{i,1} < C_{i,2} < C_{i,3}$, indicating lower liquid diffusion resistance initially and higher diffusion resistance later due to adsorbent blockage.[37] These findings imply that NOR adsorption on ASB4 involves complex mechanisms like chemisorption, external diffusion and intramaterial diffusion.

3.2.5 Adsorption isotherms. Langmuir, Freundlich, and Sips isotherms models were used to fit experimental data, and the resulting adsorption isotherm parameters are provided (Table 5 and Fig. 4c). The Langmuir model suggests monolayer adsorption with an R^2 of 0.98 at 298 K, while the Freundlich model proposes multilayer adsorption on heterogeneous surfaces with an R^2 of 0.96. Both Sips and Langmuir models show high R^2 values for NOR adsorption across all temperatures (Table 5), confirming monolayer adsorption with equal site energies on ASB4.[38] The Langmuir model estimates a maximum NOR adsorption capacity of 345.7 mg g^{-1} at 298 K, surpassing other reported materials (Table S2).

3.2.6 Adsorption thermodynamic. Thermodynamic parameters, calculated using van der Hoff equations, reveal a negative ΔG value, indicating spontaneous adsorption, with ΔG's absolute value decreasing as temperature rises, suggesting reduced adsorption efficiency at higher temperatures (Fig. 4d and Table S3). Moreover, the negative ΔH (−38.52 kJ mol^{-1}) confirms the exothermic nature of the adsorption process.

Table 5 Parameters for the adsorption isotherm models

T	Langmuir				Freundlich			Sips		
	$q_{e,exp}$ ($mg\ g^{-1}$)	$q_{e,cal}$ ($mg\ g^{-1}$)	K_L ($L\ mg^{-1}$)	R^2	K_F ($(mg^{1-n}\ L^n)\ g^{-1}$)	n	R^2	K_s ($L\ g^{-1}$)	n_s ($J\ mol^{-1}\ K^{-1}$)	R^2
298 K	332.4	345.7	0.116	0.98	68.2	2.53	0.96	0.062	0.74	0.97
308 K	306.3	323.6	0.075	0.98	57.8	2.50	0.96	0.060	0.80	0.97
318 K	291.6	303.9	0.044	0.98	38.1	2.09	0.98	0.011	0.70	0.98
328 K	271.8	291.1	0.030	0.99	20.7	1.71	0.98	0.007	0.79	0.99

3.2.7 Adsorption mechanisms. In order to explore the adsorption mechanism, the ASB4 samples were characterized by FT-IR before and after adsorption (Fig. S2a). A shift in the –OH absorption peak from 3434 to 3428 cm^{-1} suggests hydrogen bonding between NOR and oxygen-containing functional groups on the surface of ASB4 after adsorption. New peaks at 1620 and 1487 cm^{-1} indicate successful NOR adsorption onto ASB4. The benzene ring in NOR facilitates strong π–π interactions with ASB4, enhancing surface affinity.[39] Raman spectra (Fig. S2b) show a decreased I_D/I_G value, confirming π–π interactions between NOR and ASB4.[24]

XPS analysis reveals F 1s peaks after adsorption, verifying NOR adsorption by ASB4 (Fig. S2c). C 1s XPS spectrum indicate shifts in C–O and C=O peaks, implying carbon group involvement in NOR removal (Fig. S2d and e). O 1s spectrum peaks at 532.1 eV and 534.6 eV, corresponding to C–O and –OH, decrease in binding energy after NOR adsorption (Fig. S2f and g). The binding energy of C–O and –OH groups decreased after NOR adsorption, indicating their involvement through hydrogen binding. This supports the mechanism of NOR adsorption by ASB4. ASB4 material, with its mesoporous structure, enhances NOR adsorption due to its large surface area and pore structure. After NOR adsorption, the S_{BET} and V_{Total} of ASB4 decreased significantly, confirming that pore-filling is the main mechanism for NOR adsorption by ASB4 (Table S4).

To assess the individual contributions of hydrogen bonding, π–π interactions, and electrostatic interactions in NOR adsorption on ASB4, a series of competitive adsorption experiments were performed. With a 5 M concentration, urea, which competes with oxygen-containing groups, caused a 13.4% decrease in NOR removal, indicating that hydrogen bonding accounts for this portion of the adsorption process (Fig. S2h). There was also a 3.6% decrease in NOR adsorption capacity in a 200 mg per L naphthalene solution due to disrupted π–π interactions (Fig. S2i). Fig. S2j illustrated that a gradual increase in NaCl concentration to 0.1 M resulted in a 7.5% decrease in the NOR removal rate. Thus, the adsorption process is primarily driven by pore filling, followed by hydrogen bonding (13.4%), and electrostatic interactions (7.5%), with π–π interactions (3.6%) being the least significant.

3.2.8 Effect of other coexisting ions and regeneration capacity of ASB4. In wastewater, ions often compete for adsorption sites. This study added ions like Na^+, K^+, Ca^{2+}, Cu^{2+}, Fe^{3+}, Zn^{2+}, CO_3^{2-}, HCO_3^-, Br^-, NO_3^-, SO_4^{2-} to assess their impact on NOR adsorption (Fig. 5a). At 10 mmol L^{-1}, these ions didn't significantly affect NOR adsorption. However, concentrations above 10 mmol L^{-1}, particularly Zn^{2+}, Ca^{2+}, Cu^{2+} and Fe^{3+}, slightly inhibited NOR adsorption due to competition for adsorption sites. This occurrence can be attributed to the negatively charged surface of ASB4 at a pH of 8, which promotes electrostatic interactions with positively charged cations. These interactions reduce the availability of active sites for NOR adsorption. Moreover, the greater the charge of the cations, the more pronounced the electrostatic attraction, thereby further inhibiting NOR removal. Despite this, NOR removal remained at 89%. The results indicate that ASB4 has a good selective adsorption capability for NOR, even in the presence of various ions.

It is evident that, at the same concentration, quinolone antibiotics (CIP and ENX) exert a more pronounced inhibitory effect on NOR removal compared to tetracycline antibiotics (TC and OTC) (Fig. S4a). This is primarily attributed to the fact that NOR itself belongs to the quinolone class, resulting in stronger competitive adsorption among molecules with similar structures and functional groups.

Regenerative capacity is crucial for assessing adsorbent lifespan. ASB4, desorbed with 1 M NaOH, was tested for NOR adsorption and desorption performance after washing and drying. As shown in Fig. 5b, NOR removal rate dropped to 95% in the second cycle and stayed above 78% after five cycles, indicating good reusability. This phenomenon is likely attributed to the incomplete desorption of NOR during the regeneration process, resulting in residual NOR molecules adhering to the active sites of the biochar. Consequently, the availability of adsorption sites in subsequent cycles is diminished, leading to a reduction in removal efficiency. In addition, as shown in Fig. 5b, the mass loss rate remains relatively low and exhibits a decreasing trend with increasing regeneration cycles. This indicates that the majority of the loss occurs during the first regeneration, while the material's structure stabilizes in subsequent cycles. The observed mass loss can be primarily

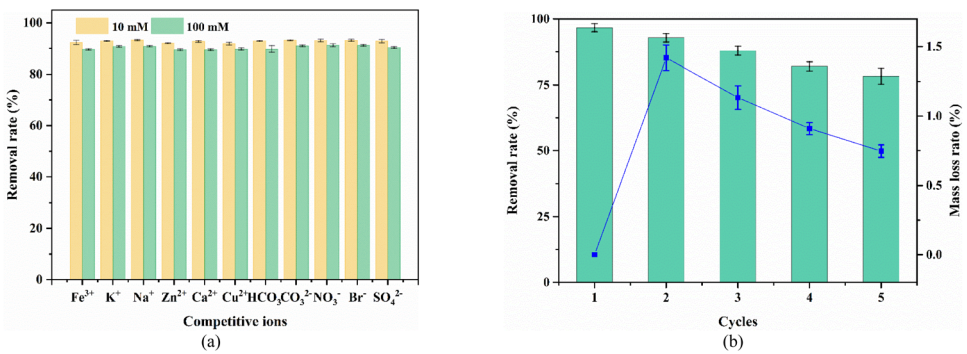

Fig. 5 Competitive effects of coexisting ions on NOR adsorption (a) and regenerative adsorption performance of ASB4 (b) (pH = 8, C_0 = 50 mg L^{-1}).

Table 6 Price comparison of ASB4 based on requirement for removal of 1 kg NOR

Adsorbent	q_e (mg g^{-1})	Req. amount (kg)	Price ($ per kg)	Total price ($ per kg)	Pay back[a] ($ per kg)
ASB4	332	3.01	2.5	7.525	1.87
Commercial biochar	66	15.15	2.5	37.88	

[a] Pay back ($ per kg): the economic benefits of producing 1 kg of ASB4 or its regenerated samples.

attributed to two factors: NaOH solution may slightly corrode the carbon framework of the biochar during regeneration and operations such as centrifugation and drying contribute to minor physical degradation.

3.2.9 Response surface regression analysis. The Box–Behnken design was used to optimize NOR adsorption conditions, with capacities ranging from 36 to 332 mg g^{-1} (Fig. S3a–c). Maximum removal capacity of 324 mg g^{-1} at a temperature of 298 K, an initial concentration of 200 mg L^{-1}, and a pH of 7.83, while strong acids, alkalis, and temperature increase negatively affected adsorption. ANOVA results (R^2 = 0.9875) indicate a strong match between predicted and experimental values (Table S5). The encoded quadratic equation for NOR adsorption is in eqn (2).

$$\begin{aligned}\text{Adsorption capacity (mg g}^{-1}) = {} & -14.28 - 0.13 \times \text{temperature} \\ & + 13.86 \times \text{pH} + 0.98 \times \text{initial concentration} \\ & - 0.03 \times \text{temperature} \times \text{pH} - 0.007 \text{ temperature} \\ & \times \text{initial concentration} \times \text{pH} + 0.002 \\ & \times \text{pH} \times \text{initial concentration} - 0.005 \\ & \times \text{temperature}^2 - 0.85 \times \text{pH}^2 + 0.003 \\ & \times \text{initial concentration}^2 \end{aligned} \quad (2)$$

3.2.10 Industrial economic feasibility analysis. A preliminary assessment of Direct Operating Costs (DOC) for producing ASB4 was conducted, focusing mainly on raw material costs due to a simple production process with minimal labor needs. ASB4 was tested alongside commercial activated carbon for wastewater treatment, showing superior adsorption capacity (332 mg g^{-1} *vs.* 66 mg g^{-1}) (Fig. S3). The estimated production cost for ASB4 is $0.62 per kg, making it more cost-effective for removing 1 kg of NOR compared to commercial adsorbents (Tables 6 and S6). ASB4 offers a potential payback of 1.87 $ per kg, highlighting its practical application potential.

4. Conclusion

In summary, a porous carbon material was prepared from AR residue using steam explosion for the treatment of NOR wastewater. The resulting biochar, ASB4, exhibits a high specific surface area of 512 m^2 g^{-1} and a total pore volume of 0.534 cm^3 g^{-1}. At 298 K, with an initial NOR concentration of 200 mg L^{-1}, ASB4 achieves a maximum adsorption capacity of 332 mg g^{-1} across a broad pH range of 2–12. The adsorption process is primarily driven by pore filling, followed by hydrogen bonding (13.4%), and electrostatic interactions (7.5%), with π–π interactions (3.6%) being the least significant. Notably, ASB4 retains over 78% NOR removal efficiency after five regeneration cycles. These findings advance our understanding of the adsorption process and mechanism of NOR adsorption on biochar produced *via* steam explosion, and they support the application of biochar in the elimination of antibiotics from wastewater.

Author contributions

Dong Guo: conceptualization, methodology, data curation, visualization, formal analysis, software, validation, writing – original draft. Pengwei Li: conceptualization, methodology, visualization, investigation, writing – review and editing. Lin Meng: conceptualization, methodology, visualization. Ziheng Zhao: conceptualization, methodology. Hang Su: conceptualization, methodology. Weisheng Feng: methodology, resources, supervision. Zhijuan Zhang: conceptualization, methodology, supervision, funding acquisition, writing – review and editing.

Conflicts of interest

The authors declare that they have no known competing financial interests or personal relationships that could have appeared to influence the work reported in this paper.

Data availability

Data will be made available on request.

Supplementary information: material characterization, adsorbent selection, FTIR spectra, Raman spectra, XPS spectra, response surface methodology analysis, competitive adsorption experiment. See DOI: **https://doi.org/10.1039/d5ra04964d**.

Acknowledgements

This work was supported by the Natural Science Foundation of Henan Province (242300420197), National Natural Science Foundation of China (No. 21878122) and Zhongjing Core Scholar's Research Initial Fund of Henan University of Chinese Medicine.

References

1 J. Wang, Q. Huang, W. Zhou, Y.-Y. Luo, J.-H. Shi, F.-X. Huang and J. Shi, *Chem. Eng. J.*, 2025, **504**, 158892.
2 X. Peng, Y. Li, Z. Jiang, K. Zhu, Q. An, Z. Xiao, X. Dong and S. Zhai, *Chem. Eng. J.*, 2024, **489**, 151263.
3 Y. Yang, Z. Zhong, J. Li, H. Du and Z. Li, *J. Hazard. Mater.*, 2022, **430**, 128500.

4 H. Yu, G. Liu, L. Shen, R. Jin, J. Zhou, H. Guo and L. Wang, *J. Hazard. Mater.*, 2023, **444**, 130394.
5 L. Chen, L. Guo, Y. Wei, G. Xiao, F. Liu, Y. Chen, X. Jin, Y. Zhu, H. Huang and Y. Lin, *J. Environ. Chem. Eng.*, 2025, **13**(5), 117454.
6 C. Pei, A. A. Aryee, K. Zhu, R. Wang and R. Han, *Sep. Purif. Technol.*, 2025, **355**, 129625.
7 J. Zhang, Y. Li, X. Wang, S. Zhao, Q. Du, X. Pi, Z. Jing and Y. Jin, *J. Colloid Interface Sci.*, 2024, **675**, 263–274.
8 Y. Li, Z. Liu, Y. Yang, H. Li, G. Qu, J. Zhao, P. Ning and K. Li, *Carbon*, 2024, **228**, 119325.
9 R. Liu, J. Song, J. Zhao, Z. Wang, J. Xu, W. Yang and J. Hu, *Chem. Eng. J.*, 2024, **497**, 154780.
10 Q. Dong, X. Min, W. Zhang, Y. Zhao and Y. Wang, *J. Hazard. Mater.*, 2024, **480**, 136202.
11 M. E. Mahmoud, N. K. Kamel, M. F. Amira and N. A. Fekry, *Sep. Purif. Technol.*, 2024, **344**, 127067.
12 S. Sağlam, F. N. Türk and H. Arslanoğlu, *Biomass Convers. Biorefin.*, 2024, **14**(9), 10791–10805.
13 K. Krysanova, A. Krylova, M. Kulikova, A. Kulikov and O. Rusakova, *Fuel*, 2022, **328**, 125220.
14 J. D. Harindintwali, C. He, L. Xiang, Q. Dou, Y. Liu, M. Wang, X. Wen, Y. Fu, M. U. Islam, S. X. Chang, S. Kueppers, S. M. Shaheen, J. Rinklebe, X. Jiang, A. Schaeffer and F. Wang, *Sci. Total Environ.*, 2023, **882**, 163643.
15 S. Kongkaew, S. Cotchim, N. Somapa, D. Somapa, R. Wannapob and W. Limbut, *Talanta*, 2026, **296**, 128387.
16 A. Averheim, G. Simões dos Reis, A. Grimm, D. Bergna, A. Heponiemi, U. Lassi and M. Thyrel, *Bioresour. Technol.*, 2024, **400**, 130698.
17 K. Poddar, D. Sarkar and A. Sarkar, *Environ. Res.*, 2024, **251**, 118711.
18 Y. Luo, J. Chen, X. Zha, J. Zhang, J. Li, G. Chen and X. He, *J. Cleaner Prod.*, 2024, **467**, 142954.
19 G. Yang, C. Pan, H. Yang and N. Feng, *BioResources*, 2021, **16**(3), 5481.
20 A. T. Hoang, X. P. Nguyen, X. Q. Duong, Ü. Ağbulut, C. Len, P. Q. P. Nguyen, M. Kchaou and W.-H. Chen, *Bioresour. Technol.*, 2023, **385**, 129398.
21 Y. Cai, Z. Si, Y. Jiang, M. Ye, F. Wang, X. Yang, J. Yu, X. Gao and W. Liu, *Carbohydr. Polym.*, 2023, **316**, 121036.
22 A. Sheik, K. Kim, G. L. Varaprasad, H. Lee, S. Kim, E. Kim, J.-Y. Shin, S. Y. Oh and Y. S. Huh, *Phytomedicine*, 2021, **91**, 153698.
23 Z. Zhao, P. Li, M. Zhang, W. Feng, H. Tang and Z. Zhang, *Environ. Res.*, 2024, **252**, 118425.
24 W. Wang, H. Shi, H. Shi, T. V. Fedorova, O. A. Glazunova, L. Mao, L. Zhang, L. Zhu, C. Wu and X. Liu, *Environ. Res.*, 2025, **285**, 122523.
25 J. Peng, F. Fan, F. Shi, J. Liu, W. Sun, Z. Huangfu, Z. Bie, Y. Jin and Y. Luo, *Sep. Purif. Technol.*, 2025, **375**, 133816.
26 G. Xiao, Q. Meng and R. Wen, *React. Funct. Polym.*, 2020, **151**, 104581.
27 P. Bhatt, Y. Huang, E. R. Rene, A. J. Kumar and S. Chen, *Bioresour. Technol.*, 2020, **305**, 123074.
28 L. Liu, X. Wang, W. Fang, X. Li, D. Shan and Y. Dai, *Environ. Res.*, 2022, **204**, 111919.
29 J. Qu, B. Zhang, H. Tong, Y. Liu, S. Wang, S. Wei, L. Wang, Y. Wang and Y. Zhang, *J. Cleaner Prod.*, 2023, **385**, 135683.
30 Q. Wang and J. Mu, *Bioresour. Technol.*, 2024, **395**, 130324.
31 X. Liu, B. Xu and J. Wang, *J. Environ. Chem. Eng.*, 2024, **12**(6), 114367.
32 B. Li, Y. Liu, W. Tong, J. Zhang, H. Tang, W. Wang, M. Gao, C. Dai, N. Liu, J. Hu and J. Li, *Bioresour. Technol.*, 2024, **413**, 131452.
33 D. Wu, Y. Fu, H. Guo, Q. Yuan, X. Nie, S. Wang and R. Gan, *Int. J. Biol. Macromol.*, 2021, **168**, 733–742.
34 Y. Lan, Y. Luo, S. Yu, H. Ye, Y. Zhang, M. Xue, Q. Sun, Z. Yin, X. Li, C. Xie, Z. Hong and B. Gao, *Sep. Purif. Technol.*, 2024, **330**, 125543.
35 H. M. Khdir and B. M. Ibrahim, *J. Mol. Liq.*, 2025, **427**, 127431.
36 G. Hong, R. Shan, J. Gu, T. Huhe, H. Yuan and Y. Chen, *J. Environ. Chem. Eng.*, 2024, **12**(2), 112208.
37 Y. Ma, T. Lu, L. Yang, L. Wu, P. Li, J. Tang, Y. Chen, F. Gao, S. Cui, X. Qi and Z. Zhang, *Environ. Pollut.*, 2022, **298**, 118833.
38 A. K. Sakhiya, V. K. Vijay and P. Kaushal, *Bioresour. Technol. Rep.*, 2022, **17**, 100920.
39 T.-K.-T. Nguyen, T.-B. Nguyen, W.-H. Chen, C.-W. Chen, A. Kumar Patel, X.-T. Bui, L. Chen, R. R. Singhania and C.-D. Dong, *Bioresour. Technol.*, 2023, **371**, 128593.